SHEAR DEFORMATION IN GRANULAR MATERIAL

S. G. Bardenhagen
Los Alamos National Laboratory
Los Alamos, NM 87545
J. U. Brackbill
Los Alamos National Laboratory
Los Alamos, NM 87545
D. L. Sulsky
University of New Mexico
Albuquerque, NM 87131

An investigation into the properties of granular materials is undertaken via numerical simulation. These simulations highlight that frictional contact, a defining characteristic of dry granular materials, and interfacial debonding, an expected deformation mode in plastic bonded explosives, must be properly modeled. Frictional contact and debonding algorithms have been implemented into FLIP, a particle in cell code, and are described. Frictionless and frictional contact are simulated, with attention paid to energy and momentum conservation. Debonding is simulated, with attention paid to the interfacial debonding speed. A first step toward calculations of shear deformation in plastic bonded explosives is made. Simulations are performed on the scale of the grains where experimental data is difficult to obtain. Two characteristics of deformation are found, namely the intermittent binding of grains when rotation and translation are insufficient to accommodate deformation, and the role of the binder as a lubricant in force chains.

INTRODUCTION

We report the results of an investigation into the micromechanical properties of granular materials, with application to plastic-bonded explosives (PBX's). PBX's are composed of polydisperse grains ranging in size from one to a few hundred micrometers, and a matrix of high-polymer binder. Low levels of applied stress sometimes cause unanticipated detonations. The inhomogeneity of the deformation at the microscale (the scale of the grains) contributes to the development of local "hot spots". If a small volume of the explosive is heated sufficiently, the consequent release of chemical energy may grow unstably and lead to detonation. Many possible mechanisms for the formation of hot spots have been proposed.[1] One explanation is that stress concentrations cause localized heating, as the volume-averaged stress is insufficient to produce significant volume-averaged heating.

Numerical simulations of the deformation of granular materials under shear are performed to gain insight into deformation modes in both dry granular materials (no interstitial material) and PBX's. The particle-in-cell (PIC) code FLIP is used to perform simulations.[2,3] The computational technique is a mix of Eulerian and Lagrangian approaches, providing a robust treatment of large deformation problems. These micromechanical simulations are on the scale of the grains, and are designed to provide insight into the nature of the deformation at the microscale. Experimental data is difficult, if not impossible, to obtain on this scale, particularly post-initiation. Of interest here is primarily mechanical behavior. Regions of high stress and large deformation indicate possible hot spot sites. This study constitutes a first step in the coupled mechanical/chemical modeling of initiation in PBX's.

Dry granular materials have many interesting properties, as they share behavior characteristic of both fluids and solids.[4] The more fluid-like regime of rapid granular flow, as may be found in grain chutes and snow avalanches, has received some attention from modelers. Grain contacts are modeled as instantaneous inelastic collisions, of varying complexity, between elastic bodies. These numerical simulations have provided insight into the microstructural character of rapid granular flow, revealing, for example, aggregation and boundary effects.[5,6] While justifiable for rapid granular flow, these models are inadequate when grain deformation is important.

For dense granular materials (large solid fraction) relative velocities of grains are small, and grains remain in contact for substantial fractions of the total loading time. In this regime incorporation of the appropriate physics requires accurate modeling of contact, frictional sliding, and the associated deformation of the grains. Powder consolidation via shock compression is an example of this deformation regime. Numerical simulations have provided insight into the microstructural character of powder compaction. The transition from "quasi-static" compaction (grain morphology remains essentially unchanged) to "dynamic" compaction (grain morphology is substantially altered by melting and "jetting") has been simulated numerically.[7,8]

Constant volume shearing of dense dry granular material provides another example of this regime. In this case the tendency of dense granular material to dilate is likely to result in large contact forces and deformations. Shearing of PBX's may be similar, but with large deformations of the soft interstitial binder also playing a role.

COMPUTATIONAL TECHNIQUE

The materials of interest include both dry granular materials, and PBX's, where an interstitial material is present. As frictional contact is the defining characteristic of dry granular materials, it is an essential ingredient in accurate modeling. Bonding is important in the case of PBX's where the binder may debond from the grains and create voids. The PIC numerical framework provides an opportunity to incorporate contact and bonding in a way which has advantages over both traditional Eulerian and Lagrangian techniques.

The fundamental idea behind the particle and cell technique used here[2,3] is that particles carry all the information required to advance the solution. The solution is advanced by interpolating particle information to a convenient computational grid (providing a cost savings as well as computational ease), solving the governing equations there, and interpolating changes back to the particles. With the updated particles reflecting current solution information (including position), the grid is discarded, and a new one used in the next computational cycle. This technique may be viewed as using Lagrangian particles to advect information through an Eulerian grid. The particles are Lagrangian material points (discretization of the problem domain is into particles, or material points) which naturally carry material properties and state variables. Advantages of this method include low diffusion and elimination of mesh tangling problems.

Natural contact algorithms exist within the particle-in-cell numerical framework, and provide some of the motivation to use the FLIP code for the numerical studies underway. The interpolation scheme used to transfer information from particles to grid provides for continuity of velocity throughout the computational domain. Consequently no two particles (initially distinct) can ever occupy the same point in space. This results in no penetration between adjacent regions of particles (i.e. bodies). Continuity of strain rate within a computational cell is another consequence. For the interpolation used here, strain rate is uniform within each cell. Regions (bodies) interact through their independent contributions to field quantities interpolated to the grid. The result is a natural no slip contact algorithm between bodies initially separated, and perfect bonding between initially adjacent bodies. The algorithm as implemented here is a uniform strain mixture theory at interfaces.

The natural contact algorithm, while limited, provides advantages over other treatments. It comes along for free with the method, unfailingly enforces no interpenetration, and requires no interface tracking. Lagrangian finite element codes require substantial additional work, including identifying contacting surfaces ahead of time, expensive search algorithms for neighboring nodes during deformation, and dependence of results on degree of interpenetration allowed.[9] Eulerian codes require substantial additional work to determine interface location and the response of mixed cells.[10]

While the natural contact algorithm is a useful one, and has allowed the study of systems in which contact is an important part,[11] it is clearly not sufficient to model frictional sliding, as is expected in the shearing of granular material. Similarly, perfect bonding is insufficient to model the decohesion of interfaces expected in the shearing of PBX's. A more general contact algorithm has been implemented in the FLIP code which incorporates Coulomb sliding friction as well as debonding. The fine points of the implementation of this algorithm are sufficiently detailed to merit a separate manuscript.[12] Only a brief overview of the algorithm and its properties is presented here.

The basic idea is to relax the single, continuous velocity field assumption inherent in the interpolation scheme from particles to grid. Rather, multiple velocity fields are allowed, one per region of particles (body). Each region is then treated with the standard numerical algorithm independently, and where velocity fields overlap (the interfaces between bodies) contact conditions are applied. The contact conditions are simply boundary conditions on the regions. This more general contact algorithm is linear in the number of grains.[12] The algorithm is general and could also be used with standard Lagrangian finite element formulations, for example.

Figure 1 gives an example of an interface vertex. The four surrounding cells and the particles in these cells are shown on the left. Quantities interpolated from the particles to the grid vertex are shown on the right. The white particles are a portion of the discretization of one region (body) and the black particles correspond to a portion of another region. When interpolated to the vertex, there is a vertex velocity corresponding to each of the regions. In addition, a center of mass velocity, v_{cm}, may be defined, which is the mass weighted average of the velocities of all particles in the vicinity. Normals may be calculated by taking the gradient of the characteristic function of each region. In addition to the quantities shown, normal tractions and bond strengths (taken to be a material property) are interpolated to the grid from the particles. These quantities allow contact to be implemented on the grid.

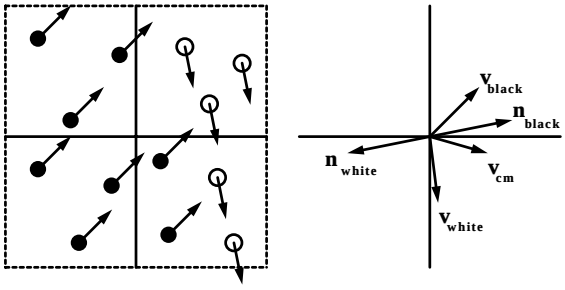

FIGURE 1. INTERFACE VERTEX, SURROUNDING MATERIAL PARTICLES, AND INTERPOLATED INTERFACE QUANTITIES.

By definition, an interface vertex is one for which v_r is different from v_{cm} for region r. Once an interface vertex has been found, the contact conditions are applied. First the normal traction is compared to the interfacial bond strength. If the normal traction exceeds the bond strength, the (vertex) bond strength is reduced, and the change interpolated to the surrounding particles. If the normal traction is positive, but less than the bond strength, then perfect bonding is enforced (a reduction to the single velocity field algorithm, i.e. $v_r = v_{cm}$).

Frictional contact occurs when the bond strength is zero and either regions are approaching or the normal traction is negative (the interface is under compression). Coulomb friction (with coefficient of sliding friction μ) is applied by calculating the angle between the interface normal and the interface velocity. If this angle is less than $\tan(\mu)$, the interface "sticks", and no-slip contact is enforced (a reduction to the single velocity field algorithm). If the angle is greater than $\tan(\mu)$ then frictional sliding occurs. Motion in the direction normal to the interface is prevented and motion tangential to the interface is reduced as required by the normal traction.

At this point frictional contact is governed by a single quantity, the coefficient of sliding friction. Normally the coefficient of static friction is somewhat larger, and introduces a further complication which has been neglected in the algorithm developed to date.

BENCHMARKING CALCULATIONS

In this section the results of two benchmarking calculations are presented. The first is for a cylinder which bounces off the computational domain boundary. Contact with the boundary represents a special case for which the contact normals can be computed exactly, eliminating a source of computational error. Two cases are presented, one for which $\mu = 0$ (frictionless contact) and the other for $\mu = .1$.

The problem is setup in arbitrary consistent units. A unit diameter cylinder is given uniform velocity with x and y components both equal to .1. The cylinder is modeled as an elastic body with bulk modulus unity, shear modulus one-half, and unit density. The magnitude of the initial velocity of the cylinder is approximately 1/8 the longitudinal wave speed (c_L=.817). Impact with the boundary results in a strong impulse, but not a strong shock. The cylinder (region) is discretized with eight cells across the diameter and 4 material points per cell.

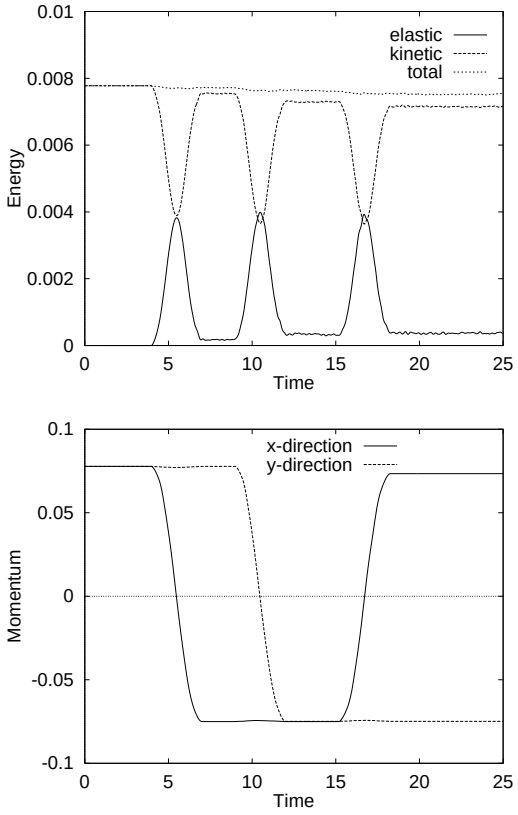

FIGURE 2. FRICTIONLESS CASE; ENERGIES AND MOMENTA OF CYLINDER THROUGHOUT THE SIMULATION.

The cylinder motion and deformation for the frictionless case is similar to that for the frictional case (as depicted in Figure 3, initial conditions are the same for both cases), but with almost no cylinder rotation. No rotation is induced by the first impact, as would be expected due to the symmetry of the initial geometry. If the cylinder were a rigid body, frictionless contact would induce no rotation for any number of impacts. However, once the cylinder begins to deform, subsequent impacts lack the symmetry required to suppress rotation. For this case the body clearly deforms (the deformation is similar to that in Figure 3), but very little rotation is induced (rotation is just perceptible after the third impact).

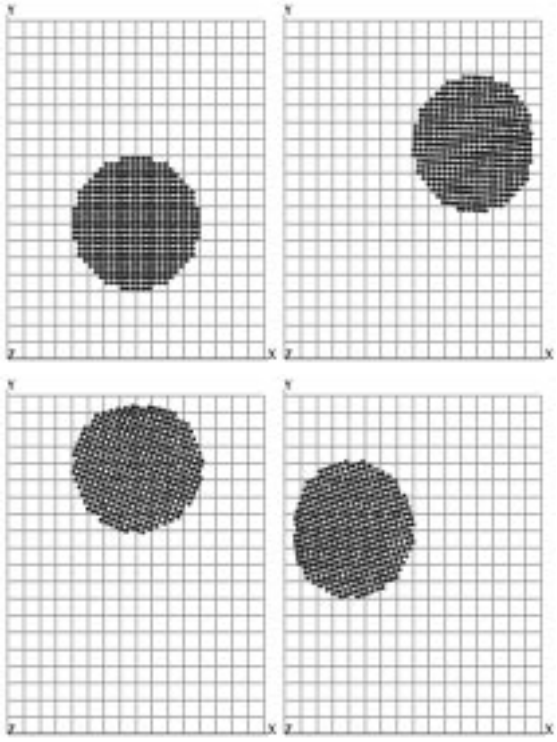

FIGURE 3. FRICTIONAL CASE; INITIAL AND IMPACTED CONFIGURATIONS OF THE CYLINDER.

Figure 2 shows energies and momenta for the frictionless boundary impact benchmarking calculation. There is no physical energy dissipation mechanism in this calculation, so the total energy (elastic plus kinetic) should remain at its initial value which is 0.0079. As can be seen from the top graph, there is some numerical dissipation, but less than 5% after 3 bounces. The dynamic exchange between elastic energy and kinetic energy during impact can be seen from the plots. All impacts have similar maxima in elastic energy. The main difference over time is that more elastic energy is stored, presumably corresponding to the increasing number of elastic waves developed with each impact. Note that this simulation is in the granular deformation regime of interest as the cylinder is in contact approximately 36% of the simulation time (12%/bounce).

The bottom graph shows momentum results. With each impact only the momentum normal to the boundary is visibly altered (consistent with the small rotations seen in the simulation). The initial value of both x and y momenta is .079. For elastic collisions the magnitude of the momentum should remain constant and equal to its initial value. Again there is some numerical dissipation. Results improve with increasing resolution.

Figure 3 shows cylinder motion and deformation for the frictional case. Both material points and

computational grid are shown. The top left frame indicates the initial configuration, where the initial velocity is directed along the line x=y. The first, second, and third impacts with the boundary are shown in the top right, bottom left, and bottom right frames respectively. For this case, substantial rotation is induced by the first impact, as is expected from the frictional forces at the boundary. There is approximately 45 degrees of rotation between the first and second impacts, and 90 degrees between the second and third.

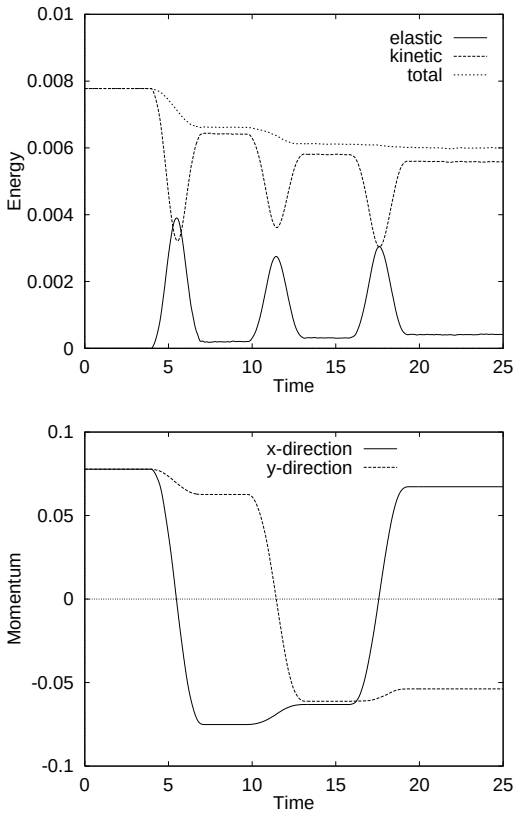

FIGURE 4. FRICTION CASE; ENERGIES AND MOMENTA OF CYLINDER THROUGHOUT THE SIMULATION.

Figure 4 shows energies and momenta for the frictional boundary impact calculation. Frictional contact dissipates energy, so the total energy decreases as seen in the top graph. Note the difference in the magnitude of the elastic energy developed in the first impact compared to subsequent ones. The first impact starts the cylinder rotating, and is more severe in the sense that it involves higher frictional forces, storing more elastic energy during contact. Subsequent impacts are less severe, the cylinder is rolling and the frictional forces aren't as large. Again more elastic energy is stored over time, presumably corresponding to elastic waves accumulating with each impact.

The bottom graph shows momentum results. With each impact the momentum tangential to the boundary is reduced (the momentum normal to the boundary changes sign, but has essentially the same magnitude, much like the frictionless case). The reduction in tangential momentum is primarily due to the frictional forces acting during contact, although some x and y momentum exchange occurs on account of the rotation induced. Again, results improve with increasing resolution.

The second benchmarking simulation is a demonstration of the debonding algorithm. The problem setup consists of two concentric cylinders subjected to a uniform, decreasing temperature. The inner cylinder is given a positive coefficient of thermal expansion. The outer cylinder, for simplicity, is given zero coefficient of thermal expansion. Decreasing the temperature causes the inner cylinder to contract, loading the outer cylinder so long as their interface remains bonded. Material properties are the same as for the contact benchmarking calculation. This calculation is more resolved than the previous one; a regular 50 x 50 grid with 4 particles per cell is used.

This problem has an analytic solution under static loading. It was found that FLIP results were very uniform, and matched the analytic solution very closely (to within a few percent for sufficiently slow temperature changes). Once the bond strength is exceeded the outer cylinder relaxes toward a completely stress free state. The inner cylinder, being thermally strained and confined out of plane, only relaxes in plane. In the absence of dissipation, elastic waves rattle around in both cylinders after the interface debonds. After a few wave transit times the solutions oscillate about the static analytical solution.

In the exact solution, debonding occurs everywhere along the interface at once. Numerically a bias is introduced due to the registry of the particles on the grid and for all calculations but one, debonding first occurred at four locations. At least four fold symmetry would be expected. However, a case was found for which the first debonding occurred at only two locations (presumably due to numerical round-off error). This case is shown in Figure 5, where the top two frames show bond strength plotted on the material particles. Medium gray corresponds to the original bond strength, black to zero. The inner and outer cylinders are distinguished by the black debonded interfacial zone and the visible gap which develops (the moire pattern is an artifact of the printing). Below each particle plot is a corresponding contour plot of the pressure distribution. These indicate both the uniformity of the solution before debonding, and the relief waves propagating outward from the interface as debonding proceeds.

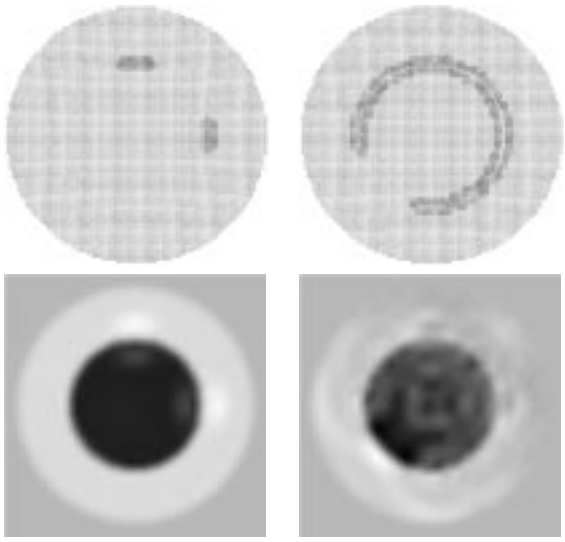

FIGURE 5. DEBONDING OF THE INTERFACE IN THE CONCENTRIC CYLINDERS PROBLEM.

The calculation shown in Figure 5 provides a chance to investigate the interfacial debonding speed. If the normal traction everywhere still bonded was infinitesimally close to the bond strength, debonding would propagate at the Rayleigh wave speed c_R (the speed of wave propagation on a free surface[13]). In the computation, the normal traction is not everywhere infinitesimally close to the bond strength, again due to the registry of a circle on a rectangular grid. The Rayleigh wave speed provides an upper bound, and it is found that the debond propagation speed is .84 c_R.

These benchmarking calculations provide assurance that the contact physics implemented can be accurately computed. The essential ingredients for numerical simulations of shear deformation in dry granular and plastic bonded granular media are in place.

NUMERICAL SIMULATIONS

Simulations of granular materials under pure shear deformation are performed in two dimensions. The simulations model large (average) shear strains (up to 100%). The simulations presented here contain only a few grains, and are not representative of the packing fractions found in PBX's. In addition the sample size is not large enough to avoid being dominated by boundary effects. These are scoping calculations. However, they exhibit behavior expected in larger samples more representative of PBX's.

Attention is paid both to the constituent properties and their interactions. Energetic crystals are modeled as elastic-plastic materials and the polymeric binder is modeled using viscoelasticity. Experimental characterization of the energetic crystals is difficult, and consequently constitutive models are difficult to calibrate. These materials have been found to fracture, although it's not clear how important this mechanism is at elevated pressures. Plasticity is believed to be a reasonable approximation to begin with. The polymeric binder, a polyurethane, has received substantial attention. A variety of experimental data is well modeled.[14] This material is well characterized over a range of strain rates for large deformations. Some work has been done to indicate appropriate frictional contact parameters.[15] A coefficient of sliding friction of .3 is used in these simulations. Bond strengths are more difficult to determine and therefore the parameters more approximate. Both zero and large bond strengths were investigated.

The initial geometry of the small granular shear simulation is depicted on the left in Figure 6. The top and bottom boundaries are periodic, so there are eleven cylinders in all. Cylinders are shaded differently only to distinguish them from one another, white space is void. Cylinders butting up against the left and right boundaries are fixed to these boundaries which have prescribed velocities and provide the shearing motion. The left boundary moves down and the right up. Calculations are on a 100 x 100 grid with 4 particles per cell.

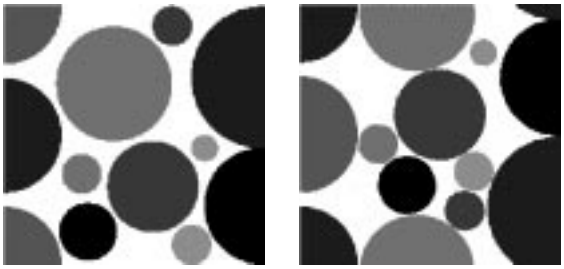

FIGURE 6. INITIAL AND FINAL GEOMETRIES FOR THE SMALL GRANULAR SHEAR PROBLEM.

Although more evident in a movie of the simulation, the middle cylinders roll and collide with each other and the boundary cylinders, but have enough room to accommodate the shearing motion without much deformation. The lack of permanent deformation is evident in the final configuration (100% shear) shown on the right in Figure 6.

Occasionally, the cylinders bind or "lock". This is seen in Figure 7, where the left frame shows cylinder positions (recall that contact is defined on the grid, so that particles one cell apart are in contact), and the right the magnitude of difference in principal stresses. This quantity is what is detected using the photoelastic technique, and used to find stress bridging, the phenomenon in granular material where chains of contacting particles transmit load.[11] Locking is a related

phenomenon occurring when the shear deformation cannot be accommodated by grain rotation and translation alone. The granular material binds and force chains develop. The diagonal of cylinders with lit up contacts in the principal stress difference plot indicates the primary load carrying path at this time.

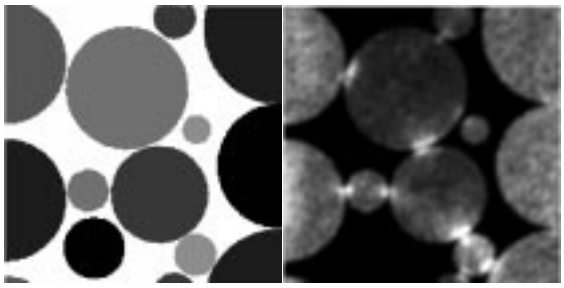

FIGURE 7. "LOCKED" STATE IN THE SMALL GRANULAR SHEAR PROBLEM.

The second simulation investigated is for the case when an interstitial material is present. The initial configuration is as Figure 6, except that all interstitial area is filled with binder. As seen in Figure 8, under the same boundary conditions cylinder translation and rotation is restrained by the presence of binder. This enhances locking, as is apparent from the deformation. The left frame is for an early time in the simulation, the right frame at the end (100% shear). Note the extensive debonding which occurs quite early in the simulation. It has been found that the extent of debonding is insensitive to bond strength over the range investigated, except in regions of continued compression (the force chain). In the force chain a large bond strength (the case depicted in Fig. 8) serves to prevent binder from squeezing out between cylinders, providing lubrication.

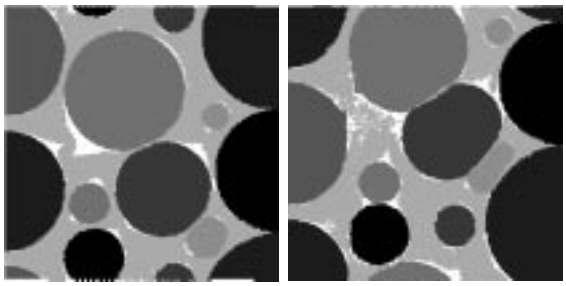

FIGURE 8. INTERMEDIATE AND FINAL STATES IN THE SHEARING OF GRAINS WITH BINDER.

It is expected that both locking and extensive debonding will occur in PBX's. In a previous study of the behavior of granular materials under (macroscopic) uniaxial strain compression, introduction of the binder was found to substantially change the behavior.[11] Computational results showed that granular material with binder under compression can behave more like a homogeneous medium. As a consequence, the stress bridging observed in the dry granular response is much reduced or absent. Under shear, however, the binder appears to have the opposite effect, and the granular material with binder may be more likely to exhibit locking than granular material without binder. The effect of bond strength on maintaining a lubricating layer of interstitial binder in force chains may also be important in PBX's.

Another phenomenon expected to be exhibited for both dry granular materials and PBX's under shear loading is shear banding. In the absence of fracture, a weak zone develops in the material after which deformation is concentrated in a region a few particles wide.[16] The reduced problems studied here have insufficient grain loading to exhibit shear banding. The next step in the investigation is to examine the response of a large collection of grains, with a high solid fraction of energetic crystals, more representative of PBX's.

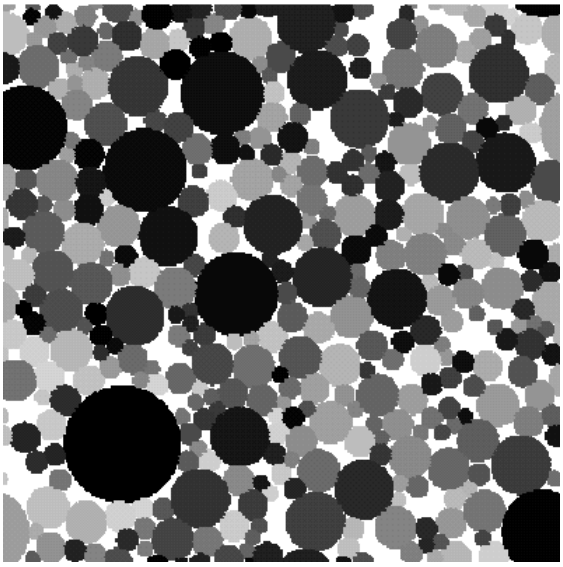

FIGURE 9. GEOMETRY APPROXIMATING THE GRAIN DISTRIBUTION IN PBX 9501.

PBX 9501 is composed of a mixture of 75% coarse and 25% fine HMX, the energetic crystal (95% by wt.), and binder (5% by wt.). The average size of the coarse crystals is approximately 150 micrometers, and the fines 5 micrometers. The typical crystal is somewhat rectangular, but with substantially rounded corners (presumably broken off during processing). However, there is also quite a bit of irregularity in crystal shapes, as some are the fusion of several (single) crystals and some are parts of fractured crystals.

The geometry depicted in Figure 9 has been chosen to approximate the energetic crystal loading and distribution found in PBX 9501. The computational domain size is 1.2 mm square. The approximation is a

two-dimensional distribution of cylinders with binder filling the interstitial areas. The distribution is chosen to represent the coarse HMX and the larger fines. The distribution of the HMX crystals covers too large a length scale range (three orders of magnitude) to include them all. Packing circles in two dimensions typically results in more void space than packing spheres in three dimensions. This is reflected in the packing density, approximately 80% by weight. The dry granular material investigated is the same cylinder distribution, but without binder. The results of this investigation are forthcoming, and are expected to bear similarities to the scoping calculations presented herein.

CONCLUSIONS

It is expected that the physical behavior exhibited by the reduced problems examined here will be born out in larger simulations, more representative of PBX's. This includes intermittent locking, and the role of binder as a lubricant in force chains. These features are expected to provide insight into possible hot spot mechanisms in PBX's during shearing deformations. Another important mechanism, shear banding, or the concentration of shear deformation in a narrow zone a few grains wide, also will be investigated with the larger sample of grains.

We expect that results in two dimensions will be confirmed by calculations in three dimensions, but three-dimensional simulations are clearly needed. The presence of a third dimension gives substantially more freedom for particles to move and relieve stress, and the geometry can only be accurately represented in three dimensions. Using the two-dimensional simulations as guides, future work includes fully three-dimensional simulations.

ACKNOWLEDGEMENTS

The authors thank Edward Kober, Group T-14, Los Alamos Nat. Lab. for developing an approximation to PBX 9501's grain distribution, and Phil Howe, DX Division, Los Alamos Nat. Lab. for helpful discussions. This work was performed under the auspices of the United States Department of Energy.

REFERENCES

1. J. E. Field, "Hot Spot Ignition Mechanisms for Explosives," Acc. Chem. Res., vol. 25, 1992, pp. 489-496.

2. J. U. Brackbill, and H. M. Ruppel, "FLIP: A Method for Adaptively-Zoned, Particle-in-Cell Calculations of Fluid Flows in Two Dimensions," J. Comput. Phys., vol 65, 1986, pp. 314-343.

3. D. Sulsky, Z. Chen, and H. L. Schreyer, "A Particle Method for History-Dependent Materials," Comp. Meth. in Appl. Mech. and Eng., vol. 118, 1994, pp. 179-196.

4. H. M. Jaeger, S. R. Nagel, and R. P. Behringer, "The Physics of Granular Materials," Phys. Today, vol. 49, 1996, pp. 32-38.

5. C. S. Campbell, and C. E. Brennen, "Computer Simulations of Granular Shear Flows," J. Fluid Mech., vol. 151, 1985, pp. 167-188.

6. A. D. Rosato, and H. Kim, "Particle Dynamics Calculations of Wall Stresses and Slip Velocities for Couette Flow of Smooth Inelastic Spheres," Continuum Mech. Thermodyn., vol. 6, 1994, pp. 1-20.

7. D. J. Benson, "An Analysis by Direct Numerical Simulation of the Effects of Particle Morphology on the Shock Compaction of Copper Powder," Modell. Simul. Mater. Sci. Eng., vol. 2, 1994, pp. 535-550.

8. D. J. Benson, V. F. Nesterenko, F. Jonsdottir, and M. A. Meyers, "Quasistatic and Dynamic Regimes of Granular Material Deformation Under Impulse Loading," J. Mech. Phys. Solids, vol. 45, 1997, pp. 1955-1999.

9. P. A. Cundall, "Formulation of a Three-Dimensional Distinct Element Method - Part I. A Scheme to Detect and Represent Contacts in a System of Many Polyhedral Blocks," Int. J. Rock. Mech. Min. Sci. & Geomech. Abstr., vol. 25, 1988, pp. 107-116.

10. D. J. Benson, "A Mixture Theory for Contact in Multimaterial Eulerian Formulations," Comp. Meth. Appl. Mech. & Eng., vol. 97, 1997, pp. 59-86.

11. S. G. Bardenhagen, and J. U. Brackbill, "Dynamic Stress Bridging in Granular Material," J. Appl. Phys., vol. 83, 1998, pp. 5732-5740.

12. S. G. Bardenhagen, J. U. Brackbill, and D. L. Sulsky, "The Material Point Method for Granular Materials," Comp. Meth. Appl. Mech. & Eng., submitted (1998).

13. H. Kolsky, **Stress Waves in Solids**, Dover, 1963.

14. S. G. Bardenhagen, E. N. Harstad, P. J. Maudlin, G. T. Gray, and J. C. Foster, "Viscoelastic Models for Explosive Binder Materials," Shock Comp. of Cond. Matter - 1997, Amherst MA, 27 Jul - 1 Aug 1997, in press.

15. J. K. A. Amuzu, B. J. Briscoe, and N. M. Chaudhri, "Frictional Properties of Explosives," J. Phys. D: Appl. Phys., vol. 9, 1976, pp. 133-143.

16. V. F. Nesterenko, M. A. Meyers, H. C. Chen, and J. C. LaSalvia, “The Structure of Controlled Shear Bands in Dynamically Deformed Reactive Mixtures,” Metallurg. and Mat. Trans. A-Phys. Metall. and Mat. Sci. vol. 26, 1995, pp. 2511-2519.